

Manipulation of Supramolecular Chirality in Bicontinuous Networks of Bent-Shaped Polycatenar Dimers

Yu Cao,^{*,[a, b, c]} Yangyang Zhao,^[a] Tianyi Tan,^[a] Feng Liu,^[a] and Mohamed Alaasar^{*,[d, e]}

Bicontinuous cubic liquid crystalline (LC) phases are of particular interest due their possible applications in electronic devices and special supramolecular chirality. Herein, we report the design and synthesis of first examples of achiral bent-shaped polycatenar dimers, capable of displaying mirror symmetry breaking in their cubic and isotropic liquid phases. The molecules have a taper-shaped 3,4,5-trialkoxybenzoate segment connected to rod-like building unit terminated with one terminal flexible chain. The two segments were connected using an aliphatic spacer with seven methylene units to induce bending of the whole structure. Investigated by the small-angle X-ray scattering (SAXS), a double network achiral cubic phase $Cub/la\bar{3}d$,

which is a *meso*-structure, and a chiral triple network cubic phase $Cub/I23^{*k}$ are formed. The molecules self-assemble into molecular helices and progress along the networks. Interestingly, different linking groups such as ester or azo linkages and core fluorination lead to distinct local helicity, resulting in an alkyl chain volume dependent phase transition sequence $la\bar{3}d(L) - I23^{*k} - la\bar{3}d(S)$. The re-entry of $la\bar{3}d$ phase and loss of supramolecular chirality is attributed to the delicate influence of steric effect at the mono-substitute end and interhelix interaction. Besides, aromatic core fluorination was proved to be a successful tool stabilizing the cubic phases in these dimers.

1. Introduction

Being a fundamental concept, chirality becomes attractive ever since its discovery by Louis Pasteur.^[1] Nowadays, chirality, serving as the basis of biological system,^[2] is also a central topic in numerous functional materials such as chiral catalysts,^[3] and chiroptical materials.^[4] Apart from functionality, material science also poses much mechanistic questions on the generation of, particularly, homochirality. Spontaneous mirror symmetry breaking is one of the chirality generation processes for achiral molecules, which was first investigated during crystallization.^[5]

To further understand the process, systems with reduced order, i.e. liquid crystals (LCs) are involved to exhibit the molecular level behaviour. Extraordinary success was achieved in bent-core molecules,^[6] dimers and trimers,^[7] and polycatenar LCs.^[8]

Polycatenar LCs consisting of a π -conjugated polyaromatic core and more than two terminal flexible chains distributed non symmetrically at both ends of the core attract particular interest.^[9] Using different building units in the backbone of these polycatenars such as azobenzene,^[10] π -conjugated [1]benzothieno[3,2-b]benzothiophene,^[11] 5,5'-diphenyl-2,2'-bithiophene^[12] or more recently the oxadiazole ring,^[13] provides wide varieties of promising functional materials for optoelectronic devices and photonic applications. In polycatenars, the aromatic cores can be packed side-by-side, forming molecular rafts with, normally, 3–6 molecules. Such rafts can further self-assembled into 2D columnar phases and 3D cubic/tetragonal/orthorhombic phases consisting networks/columns by aligning perpendicular to the columnar axis.^[14] According to present knowledge, molecular helices often formed during self-assembly to avoid clashing of alkyl chains. With proper molecular design, polycatenar molecules can overcome the helix inversion defects, creating *meso*-structure with long-range helix along 1D columns.^[14] Moreover, the system can also form homochiral phases in bicontinuous 3D phases and disorder isotropic state assigned as Iso^{*k} phase.^[8a-c,15]

Among the LC phases formed by polycatenars, two bicontinuous cubic (Cub_{bi}) phases garnered significant attention due to their complexity and generalization in various communities,^[16] beside their promising applications.^[17] Currently, the exact structures of two different types of such Cub_{bi} phases are well established, namely the *meso*-structure double network $la\bar{3}d$ phase and the chiral triple network $I23^{*k}$ phase.^[18] Both phases are formed by branched columns with three-way junctions. Junctions of networks pin the short-range helices,

[a] Y. Cao, Y. Zhao, T. Tan, F. Liu

Shaanxi International Research Center for Soft Matter, State Key Laboratory for Mechanical Behavior of Materials, Xi'an Jiaotong University, Xi'an 710049, P. R. China
E-mail: yu.cao@xjtu.edu.cn

[b] Y. Cao

Guangdong Provincial Key Laboratory of Functional and Intelligent Hybrid Materials and Devices, Guangzhou 510641, China

[c] Y. Cao

MOE Key Laboratory for Nonequilibrium Synthesis and Modulation of Condensed Matter, School of Physics, Xi'an Jiaotong University, Xi'an 710049, P. R. China

[d] M. Alaasar

Institute of Chemistry, Martin-Luther-University Halle-Wittenberg, Kurt-Mothes-Street 2, Halle 069120, Germany
E-mail: mohamed.alaasar@chemie.uni-halle.de

[e] M. Alaasar

Department of Chemistry, Faculty of Science, Cairo University, Giza 12613, Egypt

Supporting information for this article is available on the WWW under <https://doi.org/10.1002/chem.202403586>

© 2024 The Author(s). Chemistry - A European Journal published by Wiley-VCH GmbH. This is an open access article under the terms of the Creative Commons Attribution License, which permits use, distribution and reproduction in any medium, provided the original work is properly cited.

inhibiting the helix reversal to form continuous networks with homochirality. For $la\bar{3}d$ phase, two networks with opposite chirality and helix direction interwoven with each other, leading to the cancellation of chirality and formation of centrosymmetric structure.^[18a] On contrary, the $I23^{*k}$ phase with three networks forms conglomerates of chiral domains, confirmed by polarized optical microscope (POM) and circular dichroism (CD).^[8a,18b,19] Such feature makes the cubic phases perfect platform deciphering the process of chirality generation, synchronization, and their controlling factors.^[20]

Interestingly, determined by twisting angle (Φ), there're two subtypes of $la\bar{3}d$ phase with different Φ , namely, $la\bar{3}d(L)$ and $la\bar{3}d(S)$, where L and S represent the long and short helical pitch of molecular helix. Between these two $la\bar{3}d$ phases additional bicontinuous LC phases were observed, namely $I23^{*k}$ symmetry or tetragonal phases.^[15,18b] Modification of the Φ is normally achieved by alkyl chain engineering.^[9c,21] Since the twist is from aromatic core, few compounds with bent central source in their aromatic backbone were investigated aiming to control Φ value. To induce such bent in the molecular structures of polycatenars two different strategies were applied including using aliphatic spacers^[22] or a real bent-core unit such as a 4-cyanoresorcinol.^[23] However, up to date no mirror symmetry breaking was observed in LC phases exhibited by such systems, where they displayed short range of achiral cubic phases or monotropic nematic phases. Therefore, it seems that the supramolecular chirality generation remains more mystery on molecular design and self-assembly mechanism.

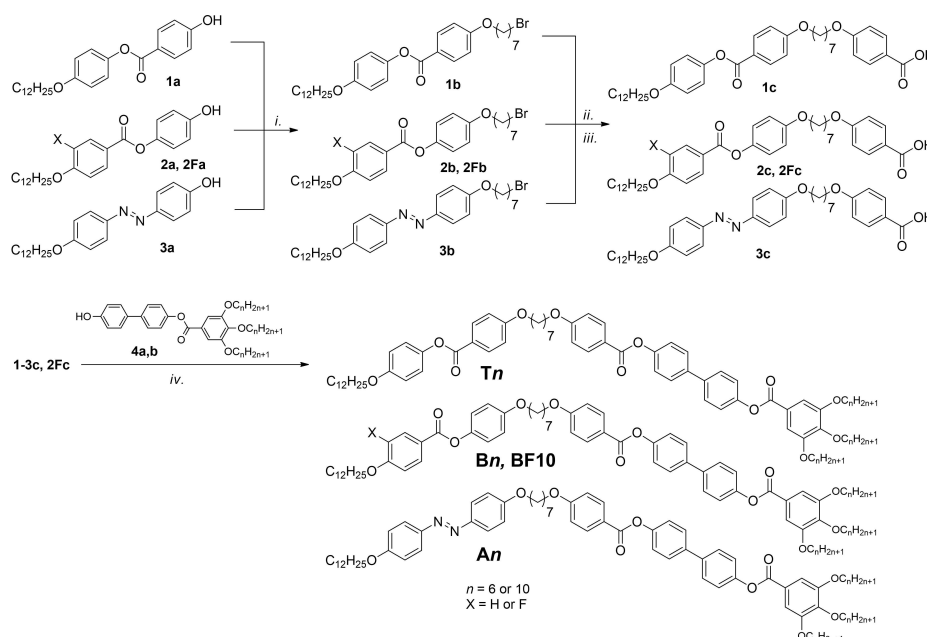
Herein, we report the first case of functional bent-shaped polycatenar dimers capable of forming mirror symmetry broken bicontinuous cubic phase ($Cub_{bi}/I23^{*k}$) as well as the two subtypes of the achiral $Cub_{bi}/la\bar{3}d$ phase ($la\bar{3}d(L)$ and $la\bar{3}d(S)$) in

relatively wide temperature ranges, making them excellent candidates for application. Chirality synchronization was also observed in their chiral isotropic liquid phases (Iso₁^[*k]). The designed materials represent dimeric molecules having two aromatic segments connected by diether linked aliphatic spacer (**Tn**, **Bn**, **BF10** and **An**, Scheme 1). The bent of the molecular structure was achieved by using a spacer with seven methylene groups in all cases. The terminal benzene ring at one end is substituted with three flexible alkoxy chains at positions 3, 4 and 5, while the other end is terminated with a dodecyloxy chain in all materials. Structural modifications were performed using different linking groups such as azo ($-N=N-$) or ester groups in the form of benzoate ($-COO-$) or with inverted direction ($-OOC-$) at the monosubstituted part. Moreover, aromatic core fluorination was used to stabilize the cubic phase.

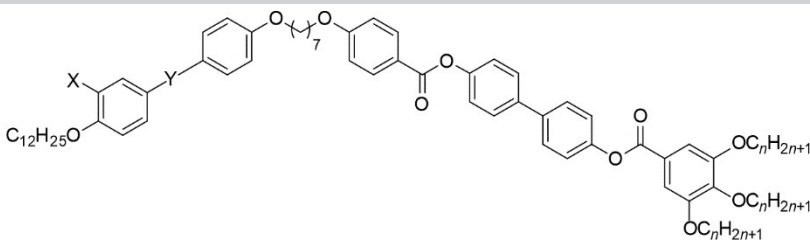
2. Synthesis

The synthesis of the target bent-shaped dimeric polycatenars (**Tn**, **Bn**, **An** and **BF10**) is illustrated in Scheme 1 and all details are given in the Supporting Information (SI) file. The final compounds are named depending on the type of the mono substituted rod-like arm, where the letters indicate the type of linking group used in this arm. Therefore, **A**=azobenzene, **B**=phenylbenzoate and **T**=inverted ester. The number of carbon atoms in each chain at the trisubstituted end is given by *n*. For compounds being fluorinated at the outer ring at the mono-substituted arm ($X=F$) F is added after the letter.

The phenolic intermediates 4-(dodecyloxy)phenyl 4-hydroxybenzoate (**1a**),^[24] 4-hydroxyphenyl 4-(dodecyloxy)benzoate



Scheme 1. Synthesis of the target dimeric polycatenars **Tn**, **Bn**, **BF10** and **An**. Reagents and conditions: *i.* 7,7'-dibromoheptane, K_2CO_3 , KI, acetone, reflux with stirring, 72 h; *ii.* 4-hydroxybenzaldehyde, K_2CO_3 , KI, acetone, reflux with stirring, 72 h; *iii.* $NaOCl_2$, NaH_2PO_4 , resorcinol, tert-butanol, stirring at RT, overnight; *iv.* $SOCl_2$, dry pyridine, triethylamine, DCM, reflux under argon atmosphere, 4 h.

Table 1. Phase transitions of compounds **Tn**, **Bn**, **An** and **BF10**.^[a]


Cpd.	X	Y	n	Phase transitions $T/^\circ\text{C}$ [$\Delta H/\text{kJ mol}^{-1}$]
T6	H	-OOC-	6	H: Cr 98 [23.2] $\text{Cub}_{\text{bi}}/Ia\bar{3}d(L)$ 142 [1.1] $\text{Iso}_1^{[*]}$ 145 [2.8] Iso C: Iso 143 [-2.8] $\text{Iso}_1^{[*]}$ 139 [-0.2] $\text{Cub}_{\text{bi}}/Ia\bar{3}d(L)$ 81 [-18.2] Cr
B6	H	-COO-	6	H: Cr 95 [47.6] $\text{Cub}_{\text{bi}}/Ia\bar{3}d(L)$ 139 [9.9] Iso C: Iso 136 [-9.7] Iso_1 135 [-1.0] $\text{Cub}_{\text{bi}}/Ia\bar{3}d(L)$ 70 [-45.3] Cr
A6	H	-N=N-	6	H: Cr 115 [33.3] $\text{Cub}_{\text{bi}}/Ia\bar{3}d(L)$ 155 [7.7] ^b Iso_1 158 [7.7] ^b Iso C: Iso 153 [-6.2] ^b Iso_1 151 [-2.5] ^b $\text{Cub}_{\text{bi}}/Ia\bar{3}d(L)$ 108 [-31.6] Cr
T10	H	-OOC-	10	H: Cr 84 [43.7] $\text{Cub}_{\text{bi}}/I23^{[*]}$ 137 ^c Mix 142 ^c $\text{Cub}_{\text{bi}}/Ia\bar{3}d(S)$ 146 [3.1] $\text{Iso}_1^{[*]}$ 149 [6.3] Iso C: Iso 147 [-6.8] $\text{Iso}_1^{[*]}$ 141 [-2.0] Mix [< 0.01] 133 ^b $\text{Cub}_{\text{bi}}/I23^{[*]}$ 59 [36.9] Cr
B10	H	-COO-	10	H: Cr 84 [25.6] $\text{Cub}_{\text{bi}}/I23^{[*]}$ 141 [7.0] Iso C: Iso 140 [-5.4] Iso_1 137 [-1.6] $\text{Cub}_{\text{bi}}/I23^{[*]}$ 53 [-23.6] Cr
A10	H	-N=N-	10	H: Cr 88 [24.2] $\text{Cub}_{\text{bi}}/I23^{[*]}$ 151 [12.6] ^b Iso_1 155 [12.6] ^b Iso C: Iso 150 [-9.7] Iso_1 146 [-2.7] $\text{Cub}_{\text{bi}}/I23^{[*]}$ 79 [-23.8] Cr
BF10	F	-COO-	10	H: Cr 80 [38.9] Cr' 90 [25.0] $\text{Cub}_{\text{bi}}/I23^{[*]}$ 128 ^c Mix [< 0.01] 134 ^c $\text{Cub}_{\text{bi}}/Ia\bar{3}d(S)$ 139 [8.1] Iso C: Iso 137 [-7.2] Iso_1 133 [-1.7] $\text{Cub}_{\text{bi}}/I23^{[*]}$ 23 [-11.7] Cr

[a] Peak temperatures as determined by DSC upon 2nd heating (H:) and 2nd cooling (C:) with a rate of 10 K min⁻¹. Abbreviations: Cr, Cr' = crystalline solid phases; Iso = isotropic liquid; $\text{Iso}_1^{[*]}$ = spontaneous symmetry broken isotropic liquid phase; Iso_1 = percolated liquid phase with network structure; $\text{Cub}_{\text{bi}}/Ia\bar{3}d(L)$ = achiral bicontinuous cubic phase with $Ia\bar{3}d$ space group and long local helical pitch; $\text{Cub}_{\text{bi}}/Ia\bar{3}d(S)$ = achiral bicontinuous cubic phase with $Ia\bar{3}d$ space group and short local helical pitch; $\text{Cub}_{\text{bi}}/I23^{[*]}$ = chiral bicontinuous cubic phase with $I23$ space group. [b] The enthalpy values cannot be separated.

(**2a**),^[25] and (E)-4-((4-(dodecyloxy)phenyl)diazenyl)phenol (**3a**),^[26] were synthesized using the same procedures reported before, while the synthesis of the fluorinated intermediate 4-hydroxyphenyl-4-(dodecyloxy)-3-fluorobenzoate (**2Fa**) is described in the SI. These intermediates were etherified with 7,7'-dibromoheptane using K_2CO_3 and a catalytic amount of KI in acetone to give the rod-like arms **1b**, **2b**, **2Fb** and **3b**. Another etherification step was performed using the obtained materials with 4-hydroxybenzaldehyde under the same conditions followed by oxidation of the obtained aldehydes using sodium chlorite (NaOCl_2) to yield the corresponding benzoic acid derivatives **1c**, **2c**, **2Fc** and **3c**. The reactive acyl chlorides of these acids was generated in the last step using SOCl_2 and a catalytic amount of *N,N*-dimethylformamide (DMF), and were then used in acylation reaction of the phenols **4a,b** to give the final bent-shaped polycatenars (**Tn**, **Bn**, **An** and **BF10**). The crude materials were purified by column chromatography using DCM as an eluent, followed by twice recrystallization from chloroform/ethanol to get the target materials. All final materials were characterized by ^1H NMR and ^{13}C NMR and elemental analysis. All synthesis details as well as all analytical data confirming the proposed molecular structures are given in the SI.

3. Results and Discussion

3.1. Thermal Behavior: DSC and POM

Primary phase investigation of the final materials was performed using POM and DSC, both on heating and cooling scans. Combined POM and DSC results for **Tn**, **Bn**, **An** and **BF10** compounds are summarized in Table 1 and represented graphically in Figure 1.

Isotropic liquid phases. All the synthesized materials except **B6** exhibit liquid-liquid transitions (Figure 1 and Table 1).

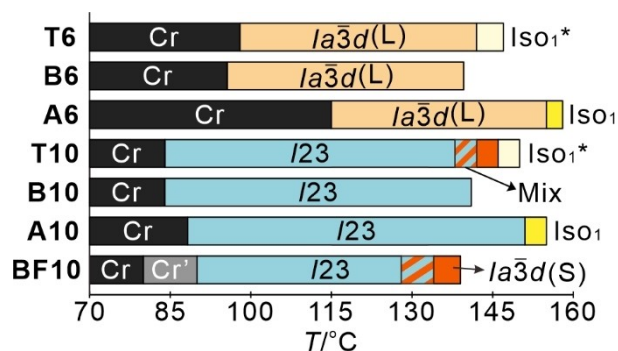


Figure 1. Phase behaviour of all soft bent-core compounds upon heating. Isotropic phase is at the right side of the bars. For abbreviations and detailed transition temperatures/enthalpies see Table 1.

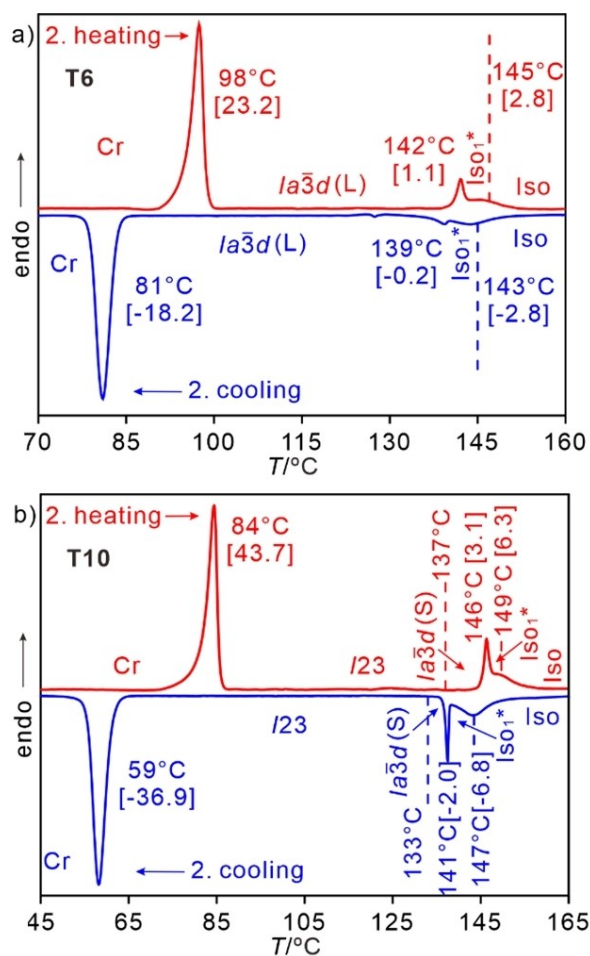


Figure 2. DSC curves during second cooling and second heating for compounds a) T6 and b) T10 with heating/cooling rate of 10 K/min.

Depending on the terminal chain length at both sides of the dimer as well as on the used linking group in the mono substituted part, this transition is either a monotropic or an enantiotropic one as recorded during DSC cooling and heating scans (Figure 2, for T6 and T10 as examples). More interesting, chiral domains could be detected in the higher temperature liquid phases (Figure 3a and b) formed by the dimers (Tn) only. Upon rotation of one polarizer with a small angle $\sim 15^\circ$ in clockwise direction from the crossed position dark and bright domains appear, which invert their sign by rotation of the analyzer in anticlockwise direction with same angle, suggesting an optically active phase of the higher temperature liquid phases of compounds T6 and T10 (Figure 3a and b). Rotation of the sample under crossed polarizer does not lead to any dark and bright domains, meaning that these observations are mainly due to the chirality instead of sample alignment.

The presence of chiral domains in these liquid phases assigned as Iso₁^[*] are due to the liquids with opposite handedness during process of pre-ordering. The formation of the Iso₁^[*] phase is accompanied with a broad transition peak on heating and cooling DSC curves, which cannot be separated from the LC phase transition i.e. Cub_{bi} - Iso₁^[*] phase transition cannot be separated (see Table 1 and Figure 2). For the achiral isotropic liquid phases assigned as Iso₁ exhibited by other dimers no chiral domains could be detected, and their formation could be observed from the DSC curves (see Figure S9 in the SI).

Unlike the Iso₁^[*] phase, formation of Iso₁ undergoes a relatively fast transition with sharper peak next to the Iso-Cub transition. The Iso₁ phases formed as metastable phases for the benzoate derived dimers (B10 and BF10) and as enantiotropic ones for the azobenzene-based dimers (A6 and A10). These chiral or achiral liquid network phases are considered as percolated liquids with dynamic helical network structures. The

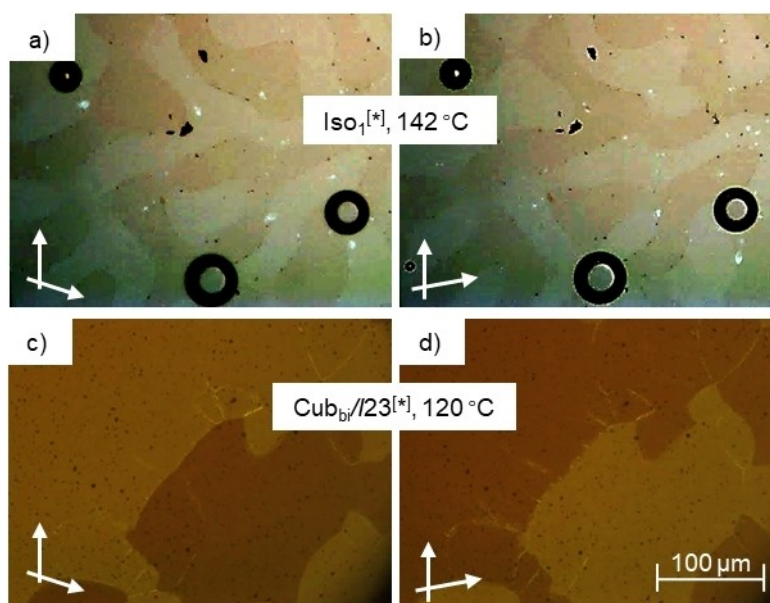


Figure 3. Optical micrographs observed on cooling in: a,b) Iso₁^[*] phase of compound T6 at 142°C and c,d) Cub_{bi}/I23^[*] phase of compound A10 at 120°C; a,c) after rotation one of the analyzers with 15° in clockwise direction and b,d) after inverting the rotation of the analyzer to be in anticlockwise direction with same angle confirming the presence of chiral domains. The scale bar in all cases is given in d).

formation of such phases is known for non-symmetric rod-like polycatenars, but those with optical activity (Iso₁^[*]) have not yet reported for any bent-shaped dimeric polycatenars.

Cubic phases. As can be seen from Table 1 and Figure 1, all synthesized materials form exclusively cubic phases. Under crossed polarizers all these phases are characterized by their isotropic appearance and their high viscosity, as typically observed for such nanostructured three-dimensional LC phases. The formation of such phases was accompanied by large enthalpy transition values (Table 1) either at the transition from the LC state to the isotropic liquid on heating (LC–Iso) or on cooling from the isotropic liquids (Iso–LC) (see Figure 2 and Figure S9 for DSC). Confirmed by POM textures, irrespective of the type of the linking group used at the mono-substituted arm (ester or azo), all materials with hexyloxy chains ($n=6$) at the crowded end do not show any optical activity.

Instead, chiral domains were observed under POM investigations as described above for the cubic phases displayed by dimers with $n=10$ (T10, B10, BF10 or A10) (e.g. Figure 3c and d). This was further confirmed by SAXS investigations (Section 3.2). Therefore, the molecular design principles represented herein successfully lead to the first examples of bent-shaped dimeric polycatenars capable of displaying mirror symmetry breaking in liquid network phases as well as in nanostructured bicontinuous cubic phases.

3.2. SAXS Investigations

To further confirm the cubic phases and to solve their exact structures, we performed SAXS investigations. Taking T10 as an example, there is only one diffused peak in WAXS pattern and centers at $d=0.45$ nm from the molten alkyl chains (Figure S13b), suggesting the LC nature of the cubic phase. The SAXS pattern of the cubic phase at 120 °C can be properly indexed as the $I23^{[*]}$ phase (Figure 4a). Reconstruction of electron density (ED) map suggests a triple network cubic bicontinuous phase (Figure 4c). Molecular rafts (Figure 4e) are perpendicular to the network in high ED region in purple and blue. A schematic figure of $I23^{[*]}$ phase with three interwoven networks is shown in Figure 4f. The inner and outer networks (pink) are same with each other except for shifting from cubic center to the vertex. And the middle network (yellow) is along the Schwarz P minimal surface. The network phase is conjugated by three-way junctions and the space group is non-centrosymmetric, leaving the $I23^{[*]}$ phase expressing chirality of molecular helices.

Upon further heating of T10 another cubic phase is formed at $T=142$ °C close to the clearing point. The SAXS pattern at 142 °C suggests an achiral $Ia\bar{3}d$ phase with typical scattering peaks in q ratio of $\sqrt{6} : \sqrt{8} : \sqrt{14} : \sqrt{16}$ (Figure 4b). The absence of chirality can also be verified by the identical POM texture upon depolarized state (Figure 4b inset). Reconstructed ED map shows the typical morphology of $Ia\bar{3}d$ phase (Figure 4d). Like $I23^{[*]}$ phase, molecular rafts are perpendicular to the network as shown in high ED region. Two chiral networks with opposite handedness can be identified in $Ia\bar{3}d$ phase,

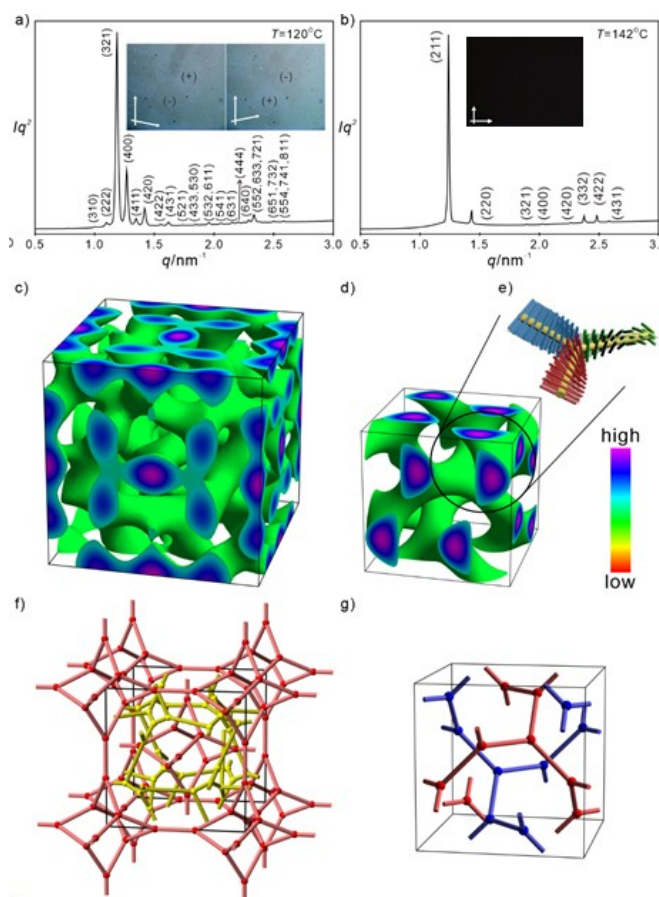


Figure 4. a) SAXS 1D diffractogram of T10 on heating at 120 °C of the $I23^{[*]}$ phase, inset: POM textures at depolarized state at $T=110$ °C, the bright and dark areas are reversed for opposite rotation direction. b) SAXS diffractogram on heating at 142 °C of the $Ia\bar{3}d(S)$ phase, inset: POM textures at depolarized state no changes for opposite rotation direction. Reconstructed ED maps of c) $I23^{[*]}$ phase and d) $Ia\bar{3}d(S)$ phase. Low electron density alkyl chains are omitted for clarity. High electron density is in purple and low is in red. e) Model of the three-way junction shows smooth progression of molecular helices at the junction. Schematic presentation of f) $I23^{[*]}$ phase and g) $Ia\bar{3}d(S)$ phase.

separated by the Gyroid minimal surface (Figure 4g). Molecular helices are also of opposite handedness, cancelling the chirality.^[18a] Thus, $Ia\bar{3}d$ phase is a *meso*-structure. Similarly, WAXS proves the fluidity of this cubic phase (Figure S8b). For other compounds, the indexation and reconstructed ED maps are essentially same, see details in Section S3.3. Interestingly, two types of $Ia\bar{3}d$ phase can be found. For $n=6$, the $Ia\bar{3}d$ phase is of large temperature range and larger lattice parameter. For $n=10$, $Ia\bar{3}d$ phase only appears at high temperature with narrow range and smaller lattice parameter (Table S8). Determined by the lattice parameter and Φ/n_{raft} , these two types of $Ia\bar{3}d$ phases are identified as $Ia\bar{3}d(S)$ and $Ia\bar{3}d(L)$, respectively. Based on the lattice parameter and network morphology, the twisting angle, Φ , number of molecules per raft, n_{raft} and twisting angle per molecule, Φ/n_{raft} can be estimated in Table 2.

Comp.	a_{cub} (nm)	a_{cub} range/nm	L_{net} (nm)	V_{cell} (nm ³)	V_{mol} (nm ³)	n_{cell}	n_{raft}	Φ ^o	Φ/n_{raft}
B6	13.18 (120 °C)	13.11–14.00	111.83	2289.5	1.714	1192.9	5.1	6.6	1.3
A6	13.13 (135 °C)	13.05–13.95	111.41	2263.6	1.709	1182.8	5.1	6.6	1.3
T6	12.48 (120 °C)	12.45–12.91	105.89	1943.8	1.714	1012.7	4.4	7.1	1.7
B10	20.79 (120 °C)	20.33–22.23	429.94	8985.9	2.161	3713.3	4.1	6.6	1.6
A10	21.20 (120 °C)	20.13–22.39	438.42	9528.1	2.157	3944.7	4.1	6.6	1.6
BF10	12.56 (133 °C)	12.56–12.56	106.57	1981.4	2.167	816.5	3.5	7.3	2.1
	19.91 (120 °C)	19.75–20.50	411.74	7892.5	2.167	3252.4	3.6	6.9	1.9
T10	12.42 (142 °C)	12.43–12.44	105.38	1915.9	2.161	791.7	3.4	7.2	2.1
	19.80 (120 °C)	19.53–20.59	409.46	7762.4	2.161	3207.7	3.6	7.0	1.9

a_{cub} = lattice parameter of cubic phase; L_{net} = total length of the networks per unit cell ($L_{\text{net}} = 8.485a_{\text{cub}}/L_{23}$, $L_{\text{net}} = 20.68a_{\text{cub}}/L_{23}$); $V_{\text{cell}} = a_{\text{cub}}^3$ = volume of the unit cell; V_{mol} = molecular volume as calculated with the crystal volume increments; n_{cell} = number of molecules in a unit cell, calculated according to $0.893 \cdot V_{\text{cell}}/V_{\text{mol}}$; n_{raft} = number of molecules organized in each 0.45 nm thick raft of the networks, calculated according to $n_{\text{raft}} = n_{\text{cell}}/(L_{\text{net}}/0.45)$; Φ = twist angle between adjacent rafts ($\Phi_{\text{I}23\text{d}} = 70.5^\circ/[0.354a_{\text{cub}}/0.45 \text{ nm}]$, $\Phi_{\text{I}23} = 90^\circ/[0.290a_{\text{cub}}/0.45 \text{ nm}]$).

3.3. Molecular Structure and Cubic Phases

In the following, discussion in the perspective of molecular shape/aromatic core is given to provide more insights into the chiral self-assembly process as well as chirality generation.

Changing the ester group direction. As shown in Scheme 1, compounds **Tn** and **Bn** are isomers differing from each other's only in the direction of the ester group. It is known from previous studies that such modification provides enhanced melting points (increased stability of crystalline phase) as well as increased clearing temperatures (LC–Iso transitions). This due to the stronger π - π stacking interactions caused by the involved electron-deficit aromatics.^[27]

Indeed, this was exactly the case for the dimeric materials **Tn** and **Bn**, where **Tn** have larger LC temperature range and higher clearing points compared to their related isomers **Bn** derivatives.

More interesting, changing the ester group direction of **B10** induces the formation of $I\bar{a}3d(S)$ in **T10**, which eliminates the supramolecular chirality. To unveil a comprehensive landscape of cubic phase transition and chirality generation, we systemically compared the Φ of different compounds. Surprisingly, the Φ of different cubic phases doesn't follow a strict trend, suggesting extra effect factor of the cubic phase transition. Instead, when considering the Φ/n_{raft} the variation becomes highly in line with phase transition (Figure 5a).

As shown in Figure 5b of the electrostatic potential map, **Tn** exhibits lower electrostatic potential at the benzene ring adjacent to the ester group in the rod-like segment. The extra $I\bar{a}3d(S)$ phase was found for **T10** at high temperature over 137 °C, where **B10** becomes Iso. As shown in Figure 5a, it's evident that compounds **Tn** has larger Φ/n_{raft} than that exhibited by the benzoate isomers **Bn**. This could be interpreted as the effect of ester group direction

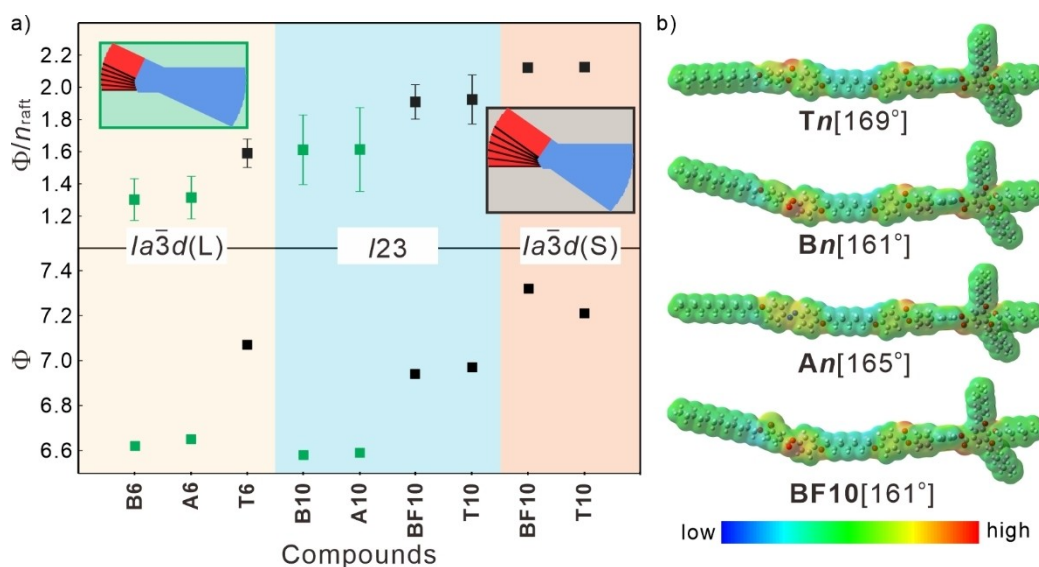


Figure 5. a) Twisting angle Φ and average Φ/n_{raft} for all compounds investigated and scheme of molecular helix of **An**, **Bn** in green and **Tn**, **BF10** in grey. b) The electrostatic potential map of four types of compounds calculated by DFT and the bent-angle value in each case between square brackets. **An**, **Bn** and **BF10** exhibit higher (light yellow) electrostatic potential in the benzene ring next to tuning group than **Tn** (light green).

represented in the models in Figure 5a. **Tn** with ester group closer to the center of molecular raft twist more to separate the neighboring ester group of high electrostatic potential.

Replacing the ester group by an azo unit. To go deeper into the influence of molecular shape on chiral self-assembly, we have also investigated the effect of replacing the ester-based wing by a more rigid and linear π -conjugated arm, namely an azobenzene-based rod-like arm (compounds **An**) on the phase behavior. DFT calculation suggests that **An** is of a bent angle $\sim 165^\circ$, just in the middle of **Tn** (169°) and **Bn** (161°) (Figure 5b). The bent-angle is a result of using a spacer with odd number of carbon atoms to connect the two aromatic segments, replacing the aromatic segments exhibits minor influence on the bent angle.^[28] As seen from Table 1 and Figure 1, the azobenzene-based materials behave very similar to **Bn** analogues with slight change in the transition temperatures. It should be noted that, similar effects were also reported in case of bent-core LCs.^[29] Thus, the bent angle is not supposed to be the main effect of cubic phase transition and chirality generation in **Tn**. On the other hand, regardless of linking group (**Tn**, **Bn**, **An**) all compounds have larger bent angle provided by the aliphatic spacer compared to that reported before in case of a real central bent-core unit such as 4-cyanoescricinol (bent angle $\sim 140^\circ$).^[28] The smaller bent angle eliminates the tendency of forming molecular helix, leading to the $la\bar{3}d(L)$ and SmA phases bent-core polycatenars, while larger bent angle in bent-shaped dimers (**Tn**, **Bn**, **An**) leads exclusively to mirror symmetry broken phases. Besides the insights about the structure-property relationships provided by using the azobenzene moiety in **An** materials, it also allows them to be used in photonic applications requiring photo-responsive materials.^[30]

Aromatic core fluorination. Peripheral aromatic fluorinated compound **BF10** was synthesized to investigate the influence of peripheral volume expansion on the LC behavior. Comparing with the neat analogue **B10**, fluorination has significant effect on the phase type and sequence (Figure 1 and Table 1). In both cases the same type of chiral $I23^{*k}$ phase was retained at low temperature but the fluorinated materials display $la\bar{3}d(S)$ phase at high temperature close to clearing point as **T10**. The lower thermal stability could be due to the steric effect of peripheral fluorine atom, resulting in less core-core interactions without disturbing the type of LC phases. Steric effect of fluorine expands the neighbouring twist and leads to a similar phase behaviour as **T10** instead of **B10**. Interestingly, **BF10** crystallizes close to room temperature (23°C), providing the potential to be used for applications at room temperature. Therefore, aromatic core fluorination can be used as an efficient tool to modify the LC phase stability in such dimeric molecules.

3.4. Mechanism of Spontaneous Chirality Generation

The comprehensive understanding of the phase behavior enables us to further explore the mechanism of spontaneous chirality generation behind the cubic phase transition. One striking question is: why **Tn** molecules exhibit an alkyl chain volume dependent phase sequence $la\bar{3}d(L) - I23^* - la\bar{3}d(S)$? Or, alter-

natively, what induces the supramolecular chirality, which stabilized the $I23^{*k}$ phase.

Upon chain elongation or heating, alkyl chain volume increases, leading to expansion of Φ/n_{raft} . The effect of space filling and interhelix interaction competes during the chiral self-assembly of the cubic phases. Overall, interhelix interaction is weak and sensitive to minor helix changes. Thus, effect of space filling serves as main factor during chiral self-assembly, i.e. $la\bar{3}d - I23^{*k}$ upon alkyl chain expansion, supported by **T6**, **A10** and **B10** with similar Φ/n_{raft} but different cubic phases. Also, the overlap of Φ/n_{raft} of **A10/B10** and **A6/B6** (green box in Figure 5a) suggests the significant effect of space filling. On the other hand, when Φ/n_{raft} increases, such overlap is largely relieved for **Tn** and **BF10**. Additionally, we calculated the dV/dr curves of the three different cubic phases (Figure 6a). Such curve describes the radial volume distribution, whose intersection with x -axis means the furthest position from the network in the lattice, i.e. minimal requirement on molecular size. Obviously, $I23^{*k}$ phase adapt molecules with long alkyl chains and $la\bar{3}d$, regardless of local twist, favors short chain.

Apart from the chain size, helix-helix interaction among molecular helices also influences the phase transition. The interhelix interaction can be tuned by temperature. In $la\bar{3}d$ phase, molecular helices are of opposite handedness along networks with opposite chirality, which indicates enantiophilic chiral self-assembly (opposite helicity along adjacent networks). This phase is proved to be able to tolerant high entropy and defects.^[31] On the other hand, $I23^{*k}$ phase, as a chiral one, exhibits same sense of molecular helix along networks, i.e. enantiophobic chiral self-assembly. Upon heating, system entropy increases, the flexible alkyl chain folding contributes more to the expansion of Φ/n_{raft} , enhancing the interhelix interaction. Besides, high temperature provides more molecular flexibility. Stronger thermal fluctuation decreases the requirement of side chain volume distribution for space filling. Interhelix interaction takes over and $I23^{*k} - la\bar{3}d$ phase transition becomes dominating,^[15] leading to a complex cubic phase sequence upon side chain volume expansion. The transition sequence of $I23^{*k} - la\bar{3}d$ phase can be further understood in the perspective of free energy $G=H-ST$ as plotted qualitatively in Figure 6b. The slope represents entropy, mainly for flexible alkyl chain conformations. The enthalpy is related to rigid core packing. Core modification could change the free energy state and change the phase transition sequence.

4. Conclusions

In summary, we reported the design and synthesis of new bent-shaped polycatenar dimers. Structural modifications were introduced using different linking groups, chaining the length of terminal flexible chain or by aromatic core fluorination. The materials exhibit two $la\bar{3}d$ phases with different local helicity ($la\bar{3}d(S)$ and $la\bar{3}d(L)$) and two symmetry broken phases ($I23^{*k}$ and Iso^{*k}). The later chiral phases have not reported before for any bent-shaped polycatenar dimers. The $la\bar{3}d(L)$ phase dominates in dimers with short alkyl chains, while $I23^{*k}$ phase is observed for longer chains. By inverting the direction of the ester group in the

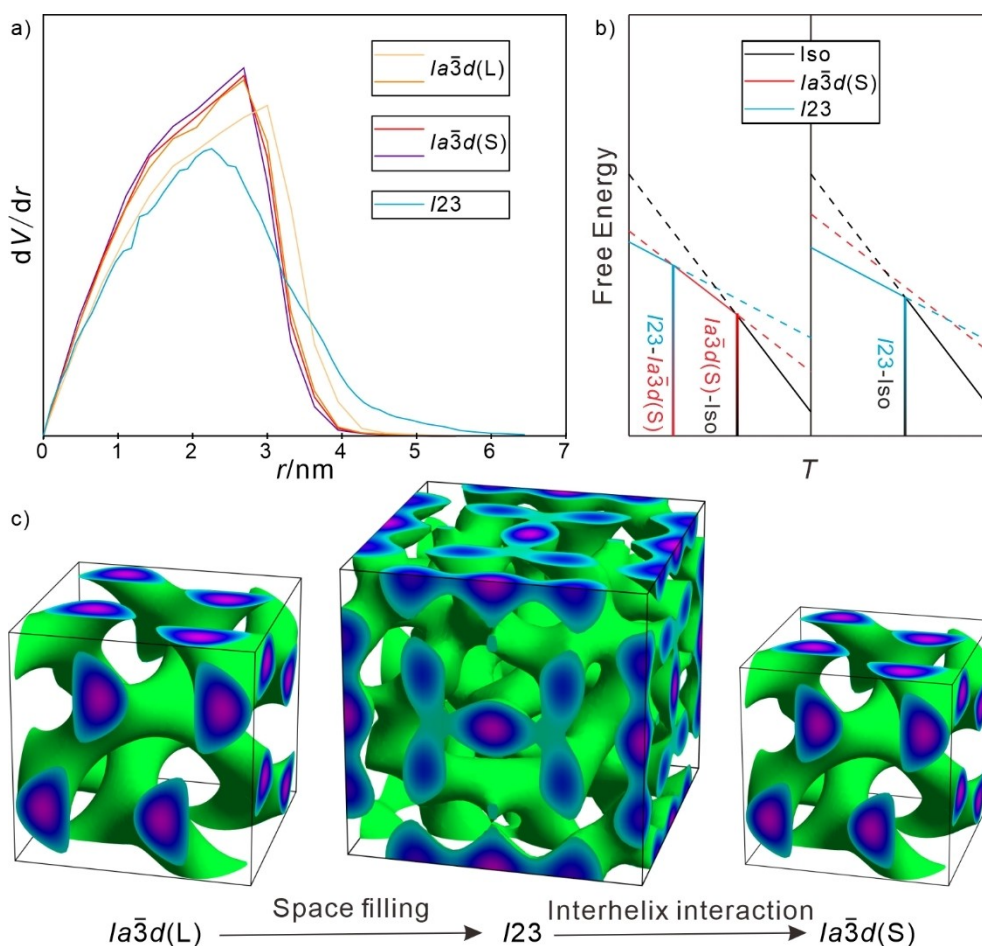


Figure 6. (a) dV/dr curve of three cubic phases. $I23^{[sk]}$ requires longest alkyl chain. (b) The qualitative free energy plots explaining the phase transition between $I23^{[sk]}$ and $Ia\bar{3}d(S)$. (c) Phase sequence among cubic phases upon side chain volume expansion and the main driving force.

rod-like wing, a phase transition between $I23^{[sk]}$ and $Ia\bar{3}d(S)$ could be achieved, which is related to the twisting angle per molecule (Φ/n_{raft}).

Overall, there is a competition for the chiral self-assembly and cubic phase transition with growing chain length, where chain elongation prefers $Ia\bar{3}d - I23^{[sk]}$ transition in the perspective of space filling. On the other hand, the interhelix interaction provides $I23^{[sk]} - Ia\bar{3}d$ transition sequence with expansion of alkyl chain volume. Our work reveals the source of $Ia\bar{3}d(L) - I23^{[sk]} - Ia\bar{3}d(S)$ transition and chirality generation upon alkyl chain volume expansion. Moreover, by tuning simultaneously the Φ/n_{raft} with aromatic core modification and alkyl chain length, more frustrated phases and novel mechanism of chirality generation might be revealed. Aromatic core fluorination leads successfully to the stabilization of the cubic phase near to room temperature, which could be of interest for potential applications.

Author Contributions

Yu Cao: Investigation, Data Curation, Visualization, Writing – review & editing, Supervision, Project administration, Funding acquisition. **Yangyang Zhao:** Investigation. **Tianyi Tan:** Inves-

tigation. **Feng Liu:** Writing – review & editing, Supervision. **Mohamed Alaasar:** Conceptualization, Investigation, Visualization, Writing – review & editing, Supervision, Project administration, Funding acquisition.

Acknowledgements

M. Alaasar acknowledges the German Research Foundation (DFG) for the financial support (AL2378/1-2, 424355983). This work is supported by the National Natural Science Foundation of China (No. 12204369), Science and Technology Agency of Shaanxi Province (2023-YBGY-459) and Guangdong Provincial Key Laboratory of Functional and Intelligent Hybrid Materials and Devices (2023-GDKLFIHMD-01). The authors thank beamlines BL16B1 at Shanghai Synchrotron Radiation Facility (SSRF) for providing the beam time. Open Access funding enabled and organized by Projekt DEAL.

Conflict of Interests

The authors declare no conflict of interest.

Data Availability Statement

Data supporting this paper, including POM textures, spectra, DSC curves and other information, is included in supporting information, which is available online or from the author.

Keywords: bent-core polycatenars · cubic network phase · chirality generation · chiral isotropic phase · gyroid

- [1] A. B. Harris, R. D. Kamien, T. C. Lubensky, *Rev. Mod. Phys.* **1999**, *71*, 1745.
 [2] J.-M. Lehn, *Angew. Chem. Int. Ed. Engl.* **1990**, *29*, 1304–1319.
 [3] T. Hashimoto, K. Maruoka, *Chem. Rev.* **2007**, *107*, 5656–5682.
 [4] a) M.-M. Zhang, K. Li, S.-Q. Zang, *Adv. Opt. Mater.* **2020**, *8*, 1902152; b) Z.-G. Zheng, Y.-Q. Lu, Q. Li, *Adv. Mater.* **2020**, *32*, 1905318; c) H. K. Bisoyi, Q. Li, *Chem. Rev.* **2022**, *122*, 4887–4926.
 [5] a) D. B. Amabilino, R. M. Kellogg, *Isr. J. Chem.* **2011**, *51*, 1034–1040; b) Y. Wang, J. Xu, Y. Wang, H. Chen, *Chem. Soc. Rev.* **2013**, *42*, 2930–2962; c) L.-C. Sögütöglu, R. R. E. Steendam, H. Meekes, E. Vlieg, F. P. J. T. Rutjes, *Chem. Soc. Rev.* **2015**, *44*, 6723–6732; d) E. Yashima, N. Ousaka, D. Taura, K. Shimomura, T. Ikai, K. Maeda, *Chem. Rev.* **2016**, *116*, 13752–13990.
 [6] a) R. A. Reddy, C. Tschierske, *J. Mater. Chem.* **2006**, *16*, 907–961; b) H. Takezoe, Y. Takahashi, *Jpn. J. Appl. Phys.* **2006**, *45*, 597; c) J. Etxebarria, M. Blanca Ros, *J. Mater. Chem.* **2008**, *18*, 2919–2926; d) L. E. Hough, H. T. Jung, D. Kruecker, M. S. Heberling, M. Nakata, C. D. Jones, D. Chen, D. R. Link, J. Zasadzinski, G. Heppke, J. P. Rabe, W. Stocker, E. Koerblova, D. M. Walba, M. A. Glaser, N. A. Clark, *Science* **2009**, *325*, 456–460; e) C. Zhang, N. Diorio, O. Lavrentovich, A. Jáklí, *Nat. Commun.* **2014**, *5*, 1–6; f) D. Chen, M. R. Tuchband, B. Horanyi, E. Koerblova, D. M. Walba, M. A. Glaser, J. E. MacLennan, N. A. Clark, *Nat. Commun.* **2015**, *6*, 1–10; g) C. Tschierske, G. Ungar, *ChemPhysChem* **2016**, *17*, 9–26; h) M. Alaasar, *Liq. Cryst.* **2016**, *43*, 2208–2243.
 [7] a) V. Borshch, Y.-K. Kim, J. Xiang, M. Gao, A. Jáklí, V. P. Panov, J. K. Vij, C. T. Imrie, M.-G. Tamba, G. H. Mehl, *Nat. Commun.* **2013**, *4*, 2635; b) R. Oikawa, H. Sasaki, Y. Takahashi, M. Sagisaka, J. Yamamoto, A. Yoshizawa, *Soft Matter* **2019**, *15*, 3179–3187; c) M. R. Tuchband, D. A. Paterson, M. Salamończyk, V. A. Norman, A. N. Scarbrough, E. Forsyth, E. Garcia, C. Wang, J. M. Storey, D. M. Walba, S. Sprunt, A. Jakli, C. Zhu, C. T. Imrie and N. A. Clark, *Proc. Natl. Acad. Sci.* **2019**, *116*, 10698–10704; d) Y. Cao, J. Feng, A. Nallapaneni, Y. Arakawa, K. Zhao, H. Zhang, G. H. Mehl, C. Zhu, F. Liu, *J. Mater. Chem. C* **2021**, *9*, 10020–10028; e) M. M. Majewska, E. Forsyth, D. Pocięcha, C. Wang, J. M. D. Storey, C. T. Imrie, E. Gorecka, *Chem. Commun.* **2022**, *58*, 5285–5288.
 [8] a) C. Dressel, F. Liu, M. Prehm, X. Zeng, G. Ungar, C. Tschierske, *Angew. Chem. Int. Ed.* **2014**, *53*, 13115–13120; b) C. Dressel, T. Reppe, M. Prehm, M. Brautzsch, C. Tschierske, *Nat. Chem.* **2014**, *6*, 971–977; c) C. Dressel, W. Weissflog, C. Tschierske, *Chem. Commun.* **2015**, *51*, 15850–15853; d) Q. Sallembien, L. Bouteiller, J. Crassous, M. Raynal, *Chem. Soc. Rev.* **2022**, *51*, 3436–3476.
 [9] a) C. Dressel, T. Reppe, S. Poppe, M. Prehm, H. Lu, X. Zeng, G. Ungar, C. Tschierske, *Adv. Funct. Mater.* **2020**, *30*, 2004353; b) T. Reppe, S. Poppe, X. Cai, Y. Cao, F. Liu, C. Tschierske, *Chem. Sci.* **2020**, *11*, 5902–5908; c) M. Alaasar, A. F. Darweesh, X. Cai, F. Liu, C. Tschierske, *Chem. Eur. J.* **2021**, *27*, 14921–14930.
 [10] a) M. Alaasar, S. Poppe, Q. Dong, F. Liu, C. Tschierske, *Chem. Commun.* **2016**, *52*, 13869–13872; b) M. Alaasar, M. Prehm, Y. Cao, F. Liu, C. Tschierske, *Angew. Chem. Int. Ed.* **2016**, *55*, 312–316; c) M. Alaasar, S. Poppe, Q. Dong, F. Liu, C. Tschierske, *Angew. Chem. Int. Ed.* **2017**, *56*, 10801–10805; d) M. Alaasar, J.-C. Schmidt, X. Cai, F. Liu, C. Tschierske, *J. Mol. Liq.* **2021**, *332*, 115870.
 [11] a) O. Kwon, X. Cai, W. Qu, F. Liu, J. Szydłowska, E. Gorecka, M. J. Han, D. K. Yoon, S. Poppe, C. Tschierske, *Adv. Funct. Mater.* **2021**, *31*, 2102271; b) O. Kwon, X. Cai, A. Saeed, F. Liu, S. Poppe, C. Tschierske, *Chem. Commun.* **2021**, *57*, 6491–6494.
 [12] M. Alaasar, A. F. Darweesh, C. Anders, K. Iakoubovskii, M. Yoshio, *Mater. Adv.* **2024**, *5*, 561–569.
 [13] M. Alaasar, A. F. Darweesh, Y. Cao, K. Iakoubovskii, M. Yoshio, *J. Mater. Chem. C* **2024**, *12*, 1523–1532.
 [14] a) Y.-x. Li, H.-f. Gao, R.-b. Zhang, K. Gabana, Q. Chang, G. A. Gehring, X.-h. Cheng, X.-b. Zeng, G. Ungar, *Nat. Commun.* **2022**, *13*, 384; b) Y. Wang, Y.-X. Li, L. Cseh, Y.-X. Chen, S.-G. Yang, X. Zeng, F. Liu, W. Hu, G. Ungar, *J. Am. Chem. Soc.* **2023**, *145*, 17443–17460.
 [15] Y. Cao, M. Alaasar, L. Zhang, C. Zhu, C. Tschierske, F. Liu, *J. Am. Chem. Soc.* **2022**, *144*, 6936–6945.
 [16] a) V. Percec, M. Peterca, T. Tadjiev, X. Zeng, G. Ungar, P. Leowanawat, E. Aqad, M. R. Imam, B. M. Rosen, U. Akbey, R. Graf, S. Sekharan, D. Sebastiani, H. W. Spiess, P. A. Heiney, S. D. Hudson, *J. Am. Chem. Soc.* **2011**, *133*, 12197–12219; b) C. Roche, H.-J. Sun, M. E. Prendergast, P. Leowanawat, B. E. Partridge, P. A. Heiney, F. Araoka, R. Graf, H. W. Spiess, X. Zeng, G. Ungar, V. Percec, *J. Am. Chem. Soc.* **2014**, *136*, 7169–7185.
 [17] S. Kutsumizu, *Isr. J. Chem.* **2012**, *52*, 844–853.
 [18] a) Y. Cao, M. Alaasar, A. Nallapaneni, M. Salamończyk, P. Marinko, E. Gorecka, C. Tschierske, F. Liu, N. Vaupotič, C. Zhu, *Phys. Rev. Lett.* **2020**, *125*, 027801; b) X. Zeng, G. Ungar, *J. Mater. Chem. C* **2020**, *8*, 5389–5398.
 [19] a) K. Ozawa, Y. Yamamura, S. Yasuzuka, H. Mori, S. Kutsumizu, K. Saito, *J. Phys. Chem. B* **2008**, *112*, 12179–12181; b) S. Kutsumizu, S. Miisako, Y. Miwa, M. Kitagawa, Y. Yamamura, K. Saito, *Phys. Chem. Chem. Phys.* **2016**, *18*, 17341–17344; c) N. Vaupotič, M. Salamończyk, J. Matraszek, M. Vogrin, D. Pocięcha, E. Gorecka, *Phys. Chem. Chem. Phys.* **2020**, *22*, 12814–12820.
 [20] a) M. Alaasar, S. Poppe, Y. Cao, C. Chen, F. Liu, C. Zhu, C. Tschierske, *J. Mater. Chem. C* **2020**, *8*, 12902–12916; b) M. Alaasar, Y. Cao, Y. Liu, F. Liu, C. Tschierske, *Chem. Eur. J.* **2022**, *28*, e202201857.
 [21] a) T. Reppe, S. Poppe, C. Tschierske, *Chem. Eur. J.* **2020**, *26*, 16066–16079; b) M. Alaasar, X. Cai, F. Kraus, M. Giese, F. Liu, C. Tschierske, *J. Mol. Liq.* **2022**, *351*, 118597.
 [22] a) J. M. Wolska, N. Topnani, E. Gorecka, J. Mieczkowski, D. Pocięcha, *ChemPhysChem* **2016**, *17*, 2686–2690; b) M. Alaasar, C. Tschierske, *Liq. Cryst.* **2017**, *44*, 387–393.
 [23] a) M. Alaasar, X. Cai, Y. Cao, F. Liu, *New J. Chem.* **2022**, *46*, 15871–15881; b) M. Alaasar, S. Poppe, *J. Mol. Liq.* **2022**, *351*, 118613.
 [24] G. Siva Mohan Reddy, T. Narasimhaswamy, K. Mohana Raju, *New J. Chem.* **2014**, *38*, 4357–4364.
 [25] K. I. Shivakumar, D. Pocięcha, J. Szczytko, S. Kapuściński, H. Monobe, P. Kaszyński, *J. Mater. Chem. C* **2020**, *8*, 1083–1088.
 [26] E. Madihlagan, S. B. N. Z. Ngaini and G. Hegde, *J. Mol. Liq.* **2019**, *292*, 111328.
 [27] a) W. Weissflog, H. N. Shreenivasa Murthy, S. Diele, G. Pelzl, *Philosophical Transactions of the Royal Society A: Mathematical, Physical and Engineering Sciences* **2006**, *364*, 2657–2679; b) G. Pelzl, W. Weissflog, *Mesophase Behaviour at the Borderline between Calamitic and “Banana-shaped” Mesogens* (Ed: A. Ramamoorthy), Springer Netherlands, Dordrecht **2007**, 1–58; c) C. Keith, M. Prehm, Y. P. Panarin, J. K. Vij, C. Tschierske, *Chem. Commun.* **2010**, *46*, 3702–3704; d) M. Alaasar, M. Prehm, C. Tschierske, *Chem. Eur. J.* **2016**, *22*, 6583–6597.
 [28] a) R. J. Mandle, E. J. Davis, C. T. Archbold, S. J. Cowling, J. W. Goodby, *J. Mater. Chem. C* **2014**, *2*, 556–566; b) S. M. Jansze, A. Martinez-Felipe, J. M. D. Storey, A. T. M. Marcelis, C. T. Imrie, *Angew. Chem. Int. Ed.* **2015**, *54*, 643–646; c) R. J. Mandle, E. J. Davis, C. C. A. Voll, C. T. Archbold, J. W. Goodby, S. J. Cowling, *Liq. Cryst.* **2015**, *42*, 688–703; d) D. A. Paterson, J. Xiang, G. Singh, R. Walker, D. M. Agra-Kooijman, A. Martinez-Felipe, M. Gao, J. M. D. Storey, S. Kumar, O. D. Lavrentovich, C. T. Imrie, *J. Am. Chem. Soc.* **2016**, *138*, 5283–5289.
 [29] a) C. Keith, A. Lehmann, U. Baumeister, M. Prehm, C. Tschierske, *Soft Matter* **2010**, *6*, 1704–1721; b) M. Alaasar, M. Prehm, M. Nagaraj, J. K. Vij, C. Tschierske, *Adv. Mater.* **2013**, *25*, 2186–2191; c) C. Tschierske, *Liq. Cryst.* **2022**, *49*, 1043–1077.
 [30] a) L. Wang, A. M. Urbas, Q. Li, *Adv. Mater.* **2020**, *32*, 1801335; b) J. Liu, Z.-P. Song, L.-Y. Sun, B.-X. Li, Y.-Q. Lu, Q. Li, *Responsive Mater.* **2023**, *1*, e20230005; c) M. Alaasar, T. Nirgude, C. Anders, *J. Mol. Liq.* **2024**, *414*, 126174; d) Y. Zhang, Z.-G. Zheng, Q. Li, *Responsive Mater.* **2024**, *2*, e20230029.
 [31] Y. Wang, S. G. Yang, Y. X. Li, Y. Cao, F. Liu, X. B. Zeng, L. Cseh, G. Ungar, *Angew. Chem. Int. Ed.* **2024**, *63*, e202403156.

Manuscript received: September 26, 2024

Accepted manuscript online: October 21, 2024

Version of record online: November 13, 2024